

Enhanced Renewable Energy Forecasting using Context-Aware Conformal Prediction

Alireza Moradi, Mathieu Tanneau, Reza Zandehshahvar, Pascal Van Hentenryck

NSF Artificial Intelligence Institute for Advances in Optimization

H. Milton Stewart School of Industrial and Systems Engineering

Georgia Institute of Technology, Atlanta, GA, USA

alirezamoradi@gatech.edu, {mathieu.tanneau, reza, pascal.vanhentenryck}@isye.gatech.edu

Abstract—Accurate forecasting is critical for reliable power grid operations, particularly as the share of renewable generation, such as wind and solar, continues to grow. Given the inherent uncertainty and variability in renewable generation, probabilistic forecasts have become essential for informed operational decisions. However, such forecasts frequently suffer from calibration issues, potentially degrading decision-making performance. Building on recent advances in Conformal Predictions, this paper introduces a tailored calibration framework that constructs context-aware calibration sets using a novel weighting scheme. The proposed framework improves the quality of probabilistic forecasts at the site and fleet levels, as demonstrated by numerical experiments on large-scale datasets covering several systems in the United States. The results demonstrate that the proposed approach achieves higher forecast reliability and robustness for renewable energy applications compared to existing baselines.

Index Terms—Renewable Energy, Conformal Prediction, Probabilistic Forecasting, Solar Forecasting

I. INTRODUCTION AND RELATED WORKS

A. Motivation

Probabilistic forecasting plays a critical role in modern power systems as operational decisions increasingly rely on accurate predictions of demand, generation, and system conditions. The continued growth of renewable energy generation, especially wind and solar, has amplified this need as their intrinsic variability introduces substantial uncertainty into grid operations. Indeed, to ensure reliable and efficient operations, system operators must effectively quantify and manage this uncertainty. In this context, probabilistic forecasting has emerged as a cornerstone of planning, market participation, and real-time control in power systems [27, 40, 11, 12, 32]. These methods have been used for short- and long-term forecasting of wind and solar energy [28, 24, 10, 34], as well as scenario generation [15, 39, 18, 4].

Two key properties of a reliable probabilistic forecasts are: 1) *calibration*, which refers to the statistical consistency between nominal and realized coverage rates, ensuring that predicted probabilities align with observed outcomes; and 2) *efficiency*, which defines the sharpness of forecasts, measured by the tightness of prediction intervals at a given target coverage level [7, 8].

Despite the significant advances in statistical [9, 25, 5, 26], physics-based [16, 19, 38], and deep learning [13, 20, 33, 17] forecasting models, they are often miscalibrated especially in

the presence of covariate shifts and regime changes which are common in renewable energy. This leads to overconfident or underconfident predictions and can degrade downstream decisions and compromise system reliability.

This paper proposes *Context-Aware Conformal Prediction (CACP)*, a new approach based on Conformal Prediction (CP) for calibrating the outputs of probabilistic forecasting models in power systems. Given a black-box model that produces quantile-based probabilistic forecasts, *CACP* generates efficient and calibrated prediction intervals. The core novelty of *CACP* is a *context-aware weighting* mechanism, utilizing physically relevant features, that assigns higher importance to calibration samples most *similar* to the target conditions at inference time. This approach enables adaptive and reliable uncertainty quantification.

B. Literature Review

CP emerged as a promising tool for uncertainty quantification and addressing the miscalibration challenge in probabilistic forecasting, offering strong theoretical guarantees and relatively low computational overhead [30]. Using a hold-out dataset (i.e., calibration set), split CP provides a model-agnostic and distribution-free calibration mechanism that adjusts the prediction intervals to achieve a user-specified target coverage. However, conventional split CP relies on the exchangeability assumption [29], which is not valid in time series. Due to the non-stationarity and regime changes in time series, particularly in renewable energy forecasting, conventional CP approaches lead to miscoverage or overly conservative prediction intervals.[36]

Recent studies have extended CP to non-exchangeable data and in the presence of covariate shifts. For example, [6] introduces AdaptiveCP, which formulates the distribution shift as a learning problem and dynamically adjusts the target coverage rate to achieve valid coverage. EnbPI is introduced for producing prediction intervals with valid marginal guarantees, utilizing ensemble estimators and bootstrapping [35]. In [37], the authors introduce SPCI to address the non-exchangeability of time series data and producing efficient prediction intervals by adaptively re-estimating the conditional quantiles of residuals.

Weighting-based methods have been also explored to extend CP beyond exchangeable data by re-weighting the conformity

scores in the calibration data. In [29], the authors propose a weighting mechanism to address covariate shift between the training and test data. NexCP is introduced in [2], which considers a nonsymmetric algorithm that assigns higher weights to the most recent observations. In [14], the authors propose KOWCPI which learns data-driven weights for sequential data to enhance the efficiency (i.e., sharpness) while achieving valid marginal coverage. Lastly, neural network-based methods such as HopCPT [1] and CT-SSF [3] have been recently used for similarity-based sample re-weighting.

In addition to these foundational contributions, recent works have utilized CP for calibration of probabilistic forecasts in power systems. In [13], the authors introduced a method combining split CP and quantile random forests for wind power prediction. Similarly, [31] proposes an asymmetric multi-quantile approach for adjusting the prediction intervals in day-ahead wind power prediction. Also, [21] implements variants of CP frameworks, weighted CP, CP with KNN, and CP with Mondrian to form uncertainty intervals on top of point-prediction models for solar PV forecasting. These studies differ from this work in that they either rely on specific quantile-based regression models (e.g., linear baselines), were not evaluated on large-scale datasets, or did not include comparisons with comprehensive conformal prediction methods.

C. Contributions and Outline

This paper makes the following key contributions to the advancement of probabilistic forecasting and calibration for renewable energy systems:

- A novel context-aware weighted calibration strategy for renewable energy systems, *CACP*, is introduced. This approach leverages physical characteristics of the system to implement a weighted CP method specifically tailored for renewable energy forecasting.
- A dynamic re-calibration framework is introduced, enabling efficient daily adjustment of forecasts to capture dynamic and short-term variations. The approach remains lightweight due to the simple yet effective weighting mechanism of *CACP*, which ensures adaptability without significant computational overhead.
- Large-scale experiments are conducted across multiple U.S. power systems, including MISO, SPP, and ERCOT, at both site and system levels. The proposed method improves coverage by approximately 12% at the system level, while reducing or maintaining interval width, and achieves up to a 55% increase in coverage at the site level.

II. BACKGROUND MATERIAL

Given a real-valued random variable Z and $\alpha \in [0, 1]$, the α quantile of Z is denoted by $Q^\alpha(Z)$. Similarly, denote $\{(z_1, p_1), \dots, (z_n, p_n)\} = \{(z_i, p_i)\}_{i=1}^n$ as pairs of $n \in \mathbb{Z}_+$ numbers z_i and non-negative weights $p_i \geq 0$ that sum to 1. *Weighted α quantile* is then defined as:

$$Q^\alpha(\{(z_i, p_i)\}_{i=1}^n) = Q^\alpha \left(\sum_{i=1}^n p_i \delta_{z_i} \right) \quad (1)$$

where δ_x denotes the Dirac distribution concentrated at x . Note that, accordingly, $\sum_{i=1}^n p_i \delta_{z_i}$ is a discrete random variable that takes value z_i with probability p_i , $i \in \{1, \dots, n\}$. Finally, define $Q^\alpha(z_1, \dots, z_n) = Q^\alpha(\{(z_i, \frac{1}{n})\}_{i=1}^n)$.

A. Problem Definition

Consider a time series $\{(x_t, y_t)\}_{t \in \mathbb{Z}}$, where $x_t \in \mathbb{R}^F$ and $y_t \in \mathbb{R}$ denote the *covariate vector* and *target variable* at time t , respectively. The covariate vector x_t captures relevant information, see Section III-B for a detailed description of the features considered in the paper. Let \mathcal{T}_{cal} denote the set of timesteps used for calibration, and let $\mathcal{D}_{cal} = \{(x_\tau, y_\tau)\}_{\tau \in \mathcal{T}_{cal}}$ denote the corresponding calibration set. Unless specified otherwise, all time periods are hourly.

The paper assumes access to a trained probabilistic forecasting model that outputs predicted quantiles $\hat{q}_t^\alpha(x_t)$, $\alpha \in [0, 1]$. This initial model yields prediction intervals of the form

$$\hat{C}_t^\alpha(x_t) = [\hat{q}^{\alpha/2}(x_t), \hat{q}^{1-\alpha/2}(x_t)], \quad \alpha \in [0, 1]. \quad (2)$$

As will be demonstrated in the experiments of Section V, such prediction intervals are often mis-calibrated, i.e.,

$$\mathbb{P}[y_t \in \hat{C}_t^\alpha(x_t)] \neq 1 - \alpha. \quad (3)$$

The goal of the paper is to produce *calibrated* and *sharp* prediction intervals using CP theory. Namely, the proposed methodology (see Section III) produces prediction intervals of the form

$$\tilde{C}_t^\alpha(x_t) = [\tilde{q}^{\alpha/2}(x_t), \tilde{q}^{1-\alpha/2}(x_t)], \quad (4)$$

where \tilde{q} are *calibrated* quantiles obtained using CP techniques.

Remark Note that the paper's methodology is agnostic to the choice of underlying model. For instance, \hat{q} may be obtained directly from a quantile regression model, or estimated from a finite set of scenarios.

B. Conformalized Quantile Regression (CQR)

Conformalized Quantile Regression (CQR) provides a distribution-free method for calibrating predictive intervals by combining quantile regression with CP [22]. A desirable feature of CQR is that it achieves finite-sample coverage guarantees while adapting to heteroscedastic data.

The CQR methodology proceeds as follows. Let $\alpha \in [0, 1]$, and consider an initial prediction interval $\hat{C}_t^\alpha(x_t)$ of the form (2). Next, for each $\tau \in \mathcal{T}_{cal}$, define the *conformity score*

$$s_\tau = \max(\hat{q}^{\alpha/2}(x_\tau) - y_\tau, y_\tau - \hat{q}^{1-\alpha/2}(x_\tau)), \quad (5)$$

and note that $s_\tau \leq 0$ if $y_\tau \in \hat{C}_\tau^\alpha$, and $s_\tau > 0$ otherwise. The conformalized prediction interval is then given by

$$\tilde{C}_t^\alpha(x_t) = [\hat{q}^{\alpha/2}(x_t) - \hat{s}, \hat{q}^{1-\alpha/2}(x_t) + \hat{s}], \quad (6)$$

where \hat{s} is the $1-\alpha$ quantile of the conformity scores obtained from the calibration data, i.e.,

$$\hat{s} = Q^{1-\alpha}(\{s_\tau\}_{\tau \in \mathcal{T}_{cal}}). \quad (7)$$

The conformalized prediction interval $\tilde{C}_t^\alpha(x_t)$ achieves marginal coverage under exchangeability condition [22].

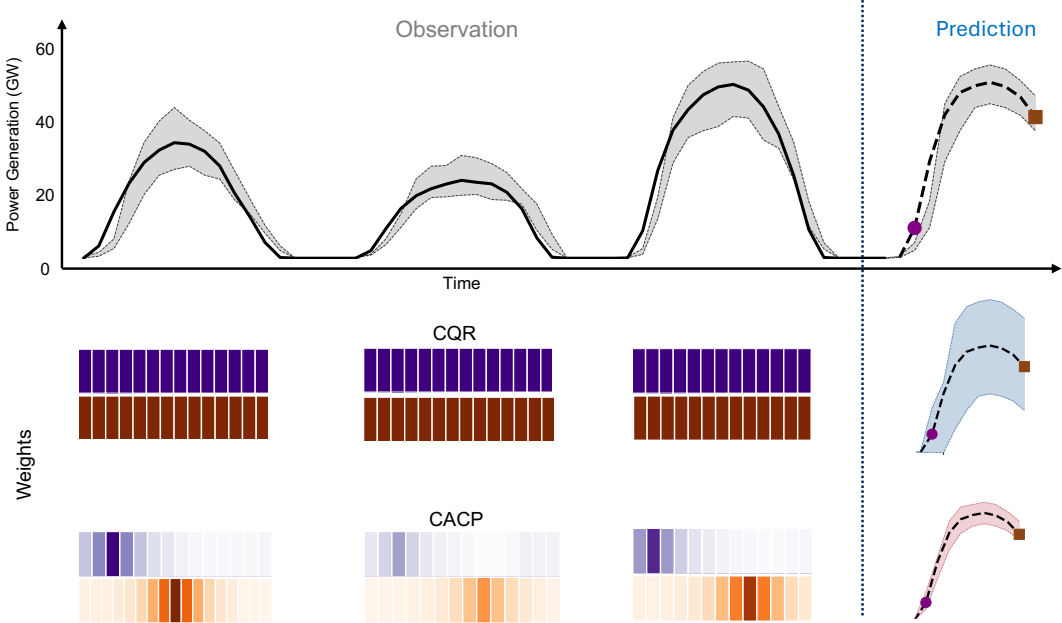


Fig. 1: Illustration of the proposed *CACP* framework. Conformity scores from the calibration set are weighted based on their similarity to the target prediction point—illustrated in purple and orange. While CQR assigns uniform weights to all samples, CACP emphasizes more *similar* instances, resulting in tighter and more efficient prediction intervals.

III. CONTEXT-AWARE CONFORMAL PREDICTION

CACP is proposed as a family of weighted conformal strategies based on physically-relevant auxiliary covariates. The central idea is to weight or restrict calibration scores based on their similarity to the target instance, thereby tailoring predictive intervals to local regimes rather than enforcing global exchangeability.

A. Weighted Conformal Prediction

The core idea of *CACP* is to re-weight the calibration scores based on a similarity metric with the test data. Let t denote the test sample, with corresponding covariate vector x_t . The method starts by computing similarity weights for each point in the calibration set, denoted by $(w_\tau)_{\tau \in \mathcal{T}_{cal}}$ and defined as

$$w_\tau = \psi(x_t, x_\tau) \geq 0, \forall \tau \in \mathcal{T}_{cal}, \quad (8)$$

where ψ is a non-negative function that computes a weight based on the similarity between the test covariates x_t and calibration covariates x_τ . Possible choices of weight function ψ are described below, and the covariates used in the paper are defined in Section III-B. The calibrated prediction interval $\tilde{C}_t^\alpha(x_t)$ is then formed using (6), where \hat{s} is computed as the weighted quantile of the conformity scores as

$$\hat{s} = Q^{1-\alpha}(\{(s_\tau, p_\tau)\}_{\tau \in \mathcal{T}_{cal}}), \quad (9)$$

and p_τ 's are obtained by normalizing the initial weights w_τ (i.e., $\sum_{\tau \in \mathcal{T}_{cal}} p_\tau = 1$). For ease of reading, the presentation of weighted CP is slightly simplified here; readers are referred to [2] for more detailed explanations.

As mentioned above, any non-negative weight function ψ may be used. Motivated by computational efficiency and interpretability, the paper considers the following three approaches:

a) Kernel: This approach computes weights based on similarity between test and calibration covariate vectors using a radial basis function (RBF) of the form

$$\psi_{RBF}(x_t, x_\tau) = \exp(-\gamma \|x_t - x_\tau\|^2), \quad (10)$$

where $\gamma > 0$ is a hyper-parameter.

b) KMeans: This approach uses a K-means algorithm to partition the calibration set $\{x_\tau\}_{\tau \in \mathcal{T}_{cal}}$ into $K \geq 0$ clusters $\mathcal{D}_1, \dots, \mathcal{D}_K$. Given a test covariate vector x_t , let κ denote the index of the cluster that contains x_t , i.e., $x_t \in \mathcal{D}_\kappa$. This yields

$$\psi_{kmeans}(x_t, x_\tau) = \begin{cases} 1 & \text{if } x_\tau \in \mathcal{D}_\kappa \\ 0 & \text{otherwise} \end{cases} \quad (11)$$

c) KNN: Given hyper-parameter $k \geq 0$, let $\mathcal{D}_K(x_t)$ denote the K -nearest neighbors of x_t in the calibration set \mathcal{D}_{cal} . Then, weights are computed as

$$\psi_{knn}(x_t, x_\tau) = \begin{cases} 1 & \text{if } x_\tau \in \mathcal{D}_K(x_t) \\ 0 & \text{otherwise} \end{cases} \quad (12)$$

B. Context-Aware Features

CACP leverages auxiliary features in the covariate vector x_t , which encode physically-relevant information. These include *historical lags* to model short-term dependencies, *time embeddings* to represent periodic temporal patterns, and *solarity* to capture daily operational cycles.

1) Historical Actuals: This feature encodes recent historical values of the actual generation to capture short-term temporal dependencies. where for an actual y_t the past k observations with a lag value l denoted as

$$H_{t,k}^l = [y_{t-l}, \dots, y_{t-l-k}]. \quad (13)$$

The lag value l ensures the usage of the actuals that are available at the time of calibration, e.g., for an observation

at the middle of the day, the actuals within the day are not accessible.

2) *Time Embeddings*: Solar generation follows well-known temporal patterns, e.g., day vs night and summer vs winter. These dynamics are captured using time embeddings:

$$\xi_t^{(v)} = (\sin \theta_t^{(v)}, \cos \theta_t^{(v)}), \quad \theta_t^{(v)} = \frac{2\pi a_t^{(v)}}{P^{(v)}}, \quad (14)$$

where $v \in \{h, d, m\}$ denotes the temporal period (hour, day, or month), and $a_t^{(h)} \in \{1, \dots, 24\}$, $a_t^{(d)} \in \{1, \dots, 365\}$, and $a_t^{(m)} \in \{1, \dots, 12\}$ represent the hour of the day, day of the year, and month of the year, respectively. The corresponding periods are $P^{(h)} = 24$, $P^{(d)} = 365$, and $P^{(m)} = 12$. Note that sin-cos embeddings are standard in Machine Learning literature for embedding temporal information, as they naturally encode the periodicity of the underlying data.

3) *Normalized Time of Solar Day*: One limitation of the time embeddings defined in Eq. (14) is that they do not explicitly capture variations in daylight throughout the year. This is especially important when considering a system comprising multiple solar sites spread across a large geographical area. To that end, the paper considers an additional embedding $\xi_t^s = (\sin \varphi_t, \cos \varphi_t)$, where $\varphi_t = 2\pi \rho_t$ and ρ_t is the *normalized time of solar day*, defined as:

$$\rho_t = \frac{t - t^{\text{sunrise}}}{t^{\text{sunset}} - t^{\text{sunrise}}} \in [0, 1], \quad (15)$$

where t denotes the current time step, and $t^{\text{sunrise}}, t^{\text{sunset}}$ denote the sunrise and sunset time at a given location, respectively. Note that this feature is only defined during daytime. When considering the total generation across the entire system, the definition above is extended by defining $t^{\text{sunrise}}, t^{\text{sunset}}$ as the earliest sunrise and latest sunset time across all solar sites.

The covariate vector x_t (same for x_τ) is then formed by concatenating the features as follows:

$$x_t = (H_{t,k}^l, \xi_t^h, \xi_t^d, \xi_t^m, \xi_t^s). \quad (16)$$

Additional covariates such as meteorological variables and solar-geometry features (e.g., solar angle) can be incorporated to further enhance predictive performance.

To ensure the intervals remain efficient and well-calibrated, the proposed method includes a hyperparameter tuning and feature selection step as part of training. This process identifies optimal hyper-parameters and the most informative subset of features based on validation performance, see Section III-C.

C. Dynamic Hypertuning and Calibration Strategy

An important contribution of the paper is a dynamic hypertuning strategy that improves adaptability to evolving temporal dynamics and potential distribution shifts in the data. Thereby, hypertuning, feature selection and model selection steps are performed periodically as follows. Let δ_{rec} denote the recalibration frequency, e.g., daily in the current work. Every δ_{rec} steps, a tuning set $\mathcal{D}_{\text{tune}}$ and validation set \mathcal{D}_{val} are formed using historical data. Note this is typically done by splitting a held-out dataset, i.e., data not used for training the

TABLE I: Method hyper-parameters and their values

Method	Parameter	Value
CQR	—	—
AdaptiveCP	γ	1e-4, 5e-4, 1e-3
NexCP	ρ	0.95, 0.98, 0.995
HopCPT	β	5.0, 10.0, 20.0
$CACP_{\text{Kmeans}}$	K	3, 5, 8, 12
$CACP_{\text{KNN}}$	K	50, 100, 200, 500, 1000
$CACP_{\text{Kernel}}$	kernel	RBF, Laplacian
$CACP_{\text{Kernel}}$	γ	0.5, 1.0, 2.0

underlying probabilistic forecasting model, into two subsets, with \mathcal{D}_{val} comprising more recent data.

For each $CACP$ model (i.e. choice of weight function ψ as described in Section III-A), hyperparameter optimization and feature selection is performed by maximizing performance on the validation set. This can be performed using exhaustive or random search, or off-the-self hypertuning tools. A core enabler of this approach is the computational efficiency of $CACP$, i.e., it is possible to re-tune models daily within a few minutes using only a CPU machine. In contrast, deep learning-based approaches like HopCPT [1] introduce multiple hyperparameters and require several GPU-hours to train, which increase computing costs and limits the ability to perform hypertuning at scale.

IV. EXPERIMENT SETUP

A. Data

Experiments are conducted on large-scale datasets covering major U.S. power systems, including the *Midcontinent Independent System Operator (MISO)*, *Southwest Power Pool (SPP)*, and the *Electric Reliability Council of Texas (ERCOT)*. The study targets day-ahead solar power generation forecasts at both site and system levels, provided by the *National Renewable Energy Laboratory (NREL)* [23]. The dataset contains hourly time series of actual and forecasts (in the form of quantiles) of solar power generation for the year 2019, consisting of a total of 1149 sites (751 for MISO, 172 for SPP, and 226 for ERCOT) and 3 systems. The calibration models take as input NREL's quantile-based forecasts, actual historical values, and context-aware features (if applicable), and produce adjusted prediction intervals.

The first two months of 2019 (upto March 1st) are used as the initial calibration set. Thereafter, the calibration models are updated daily to adjust the day-ahead forecasts. For each test day, the preceding week serves as the validation set (for parameter tuning), while calibration is performed using all data available prior to that day.

B. Baseline Methods

The results are compared with the following baselines:

- **NREL**: The raw solar power generation forecasts provided by NREL. These forecasts are provided in the

form of 99 quantiles. For each target coverage rate, the corresponding quantiles are selected.

- **CQR** [22]: Applies the CQR method using NREL's quantile-based forecasts and historical observations.
- **AdaptiveCP** [6]: This approach adjusts the target coverage rate dynamically to account for the distribution drift in the data. The original method is developed for deterministic forecasts. Here, the conformity score is adjusted using (5).
- **NexCP** [2]: This is a weighting-based CP approach, which considers higher importance to the most recent observation in the calibration data. Similar to AdaptiveCP, the conformity score in NexCP is modified to align with (5).
- **HopCPT** [1]: This approach trains a neural network to learn similarity-based weights for time series data. The Hopfield network loss function is reformulated for compatibility with quantile forecasts. Due to its high computational cost, HopCPT is evaluated only for system-level forecasts. For this approach, the loss function is defined as below:

$$\mathcal{L} = \frac{1}{|\mathcal{T}|} \| (|\mathbf{s}_{1:\mathcal{T}}| - \mathbf{A}_{\mathcal{T}} |\mathbf{s}_{1:\mathcal{T}}|)^2 \|_1, \quad (17)$$

where $\mathbf{A} \in \mathbb{R}^{\mathcal{T} \times \mathcal{T}}$ denotes the Hopfield association matrix capturing pairwise dependencies among conformity scores \mathbf{s} as defined in (5).

Table I summarizes the hyperparameters used for all methods. To balance coverage and efficiency, parameters are tuned by minimizing the **Winkler Score** (WS) as defined in (22), with the exception of HopCPT, whose hyperparameters are optimized by directly minimizing (17) over the validation data.

C. Evaluation Metrics

The performance of each method is evaluated using three standard metrics. Let $\mathcal{T}_{\text{test}}$ denote the set of all time indices in the test set, with size $|\mathcal{T}_{\text{test}}|$. Given the target value y_t (for some $t \in \mathcal{T}_{\text{test}}$) and the predicted interval $\hat{C}_t^\alpha = [\hat{C}_t^{\alpha,l}, \hat{C}_t^{\alpha,u}]$, the metrics are defined as follows:

a) Prediction Interval Coverage Probability (PICP):

This metric measures the empirical coverage rate of the prediction intervals and is defined as follows:

$$\text{PICP}^\alpha = \frac{1}{|\mathcal{T}_{\text{test}}|} \sum_{t \in \mathcal{T}_{\text{test}}} \mathbf{1}\{y_t \in \hat{C}_t^\alpha\}, \quad (18)$$

b) Average Interval Width (AIW): This metric evaluates the sharpness of the prediction intervals at a given target coverage level, α , and is defined as:

$$\text{AIW}^\alpha = \frac{1}{|\mathcal{T}_{\text{test}}|} \sum_{t \in \mathcal{T}_{\text{test}}} \text{IW}_t^\alpha, \quad (19)$$

$$\text{IW}_t^\alpha = \hat{C}_t^{\alpha,u} - \hat{C}_t^{\alpha,l} \quad (20)$$

c) Winkler Score (WS): This metric combines PICP and AIW and is defined as:

$$\text{WS}^\alpha = \frac{1}{|\mathcal{T}_{\text{test}}|} \sum_{t \in \mathcal{T}_{\text{test}}} \text{WS}_t^\alpha \quad (21)$$

where,

$$\text{WS}_t^\alpha = \begin{cases} \text{IW}_t^\alpha + \frac{2}{\alpha}(y_t - \hat{C}_t^{\alpha,u}), & y_t > \hat{C}_t^{\alpha,u}, \\ \text{IW}_t^\alpha + \frac{2}{\alpha}(\hat{C}_t^{\alpha,l} - y_t), & y_t < \hat{C}_t^{\alpha,l}, \\ \text{IW}_t^\alpha, & \text{otherwise.} \end{cases} \quad (22)$$

For site-level experiments, all metrics are computed per site and then averaged across all sites that are within the same system. All time series are normalized by the maximum capacity of their corresponding systems or sites.

V. NUMERICAL RESULTS

A. Results Analysis

Tables II and III present the system- and site-level results, respectively. The average PICP^α , AIW^α , and WS^α values are provided for the proposed method and baselines for MISO, ERCOT, and SPP. The target coverages are considered as 90%, 80%, 70%, 60% (i.e., $\alpha = 0.1, 0.2, 0.3, 0.4$), and the superscripts are omitted unless stated otherwise. All metrics are computed over daylight hours, corresponding to periods with nonzero solar generation. Note that HopCPT is evaluated only for system-level calibration due to the prohibitive computational cost of training across a large number of sites.

The results indicate that the NREL probabilistic forecasts exhibit miscoverage rates ranging from approximately 17% to 22.5% at the system level, and from 28% to 52.1% at the site level at 90% coverage (see Table III and II). The substantially lower coverage at the site level highlights the increased difficulty of forecasting at a high granularity level, due to higher local variability. All CP methods substantially improve the PICP, achieving empirical coverage close to the 90% target, while maintaining or even reducing the AIWs at both system- and site-level forecasts. This includes the basic CQR approach, which does not include any covariates or context-aware weighting mechanisms. The only exception is AdaptiveCP, which improves upon NREL's raw forecasts but fails to consistently reach the target, particularly when the base forecasts are severely miscalibrated. For example, in ERCOT, NREL's PICP for 90% target coverage is 77.5% at the system level and 47.9% at the site level. After calibration with AdaptiveCP, the miscoverage remains at 3.6% and 27.23%, respectively.

Comparison with baseline methods shows that the proposed CACP-based methods consistently achieve the lowest WS for both system- and site-level forecasts, with CACP_{KNN} being the best performing model. To further illustrate the trade-off between PICP and AIW, Fig. 2 plots PICP versus AIW at various target coverage levels for all system-level forecasts. As shown, the proposed method consistently outperforms all baselines, achieving tighter intervals while maintaining valid coverage. The closest competitor is HopCPT, which has a significantly higher computational cost. Similar experiments were conducted for site-level forecasts, which showed consistent trends.

TABLE II: Average Performance across Systems (Day-Ahead Forecasts)

ISO	Method	(1- α) = 90%			(1- α) = 80%			(1- α) = 70%			(1- α) = 60%		
		PICP \uparrow	AIW \downarrow	WS \downarrow	PICP \uparrow	AIW \downarrow	WS \downarrow	PICP \uparrow	AIW \downarrow	WS \downarrow	PICP \uparrow	AIW \downarrow	WS \downarrow
ERCOT	NREL	77.50	0.1933	0.3455	71.98	0.1658	0.2531	65.21	0.1418	0.2117	58.51	0.1193	0.1839
	CQR	89.05	0.2257	0.3240	80.16	0.1741	0.2495	71.37	0.1457	0.2097	61.82	0.1193	0.1823
	AdaptiveCP	86.40	0.2121	0.3307	77.85	0.1716	0.2520	69.37	0.1446	0.2114	59.41	0.1188	0.1837
	NexCP	89.59	0.2272	0.3167	78.96	0.1739	0.2452	67.50	0.1373	0.2073	56.51	0.1081	0.1805
	HopCPT	87.50	0.2114	0.3056	78.90	0.1690	0.2382	68.75	0.1382	0.2072	60.28	0.1124	0.1832
	$CACP_{Kmeans}$	89.98	0.2144	0.2825	79.71	0.1630	0.2280	68.75	0.1294	0.1957	58.15	0.1028	0.1714
	$CACP_{KNN}$	89.36	0.2063	0.2778	80.17	0.1589	0.2222	69.58	0.1267	0.1892	58.51	0.1009	0.1659
MISO	$CACP_{Kernel}$	90.13	0.2174	0.2741	79.67	0.1650	0.2225	68.94	0.1295	0.1913	57.41	0.1016	0.1684
	NREL	82.12	0.1261	0.1386	73.01	0.0981	0.1115	66.05	0.0792	0.0945	59.47	0.0644	0.0819
	CQR	93.29	0.1298	0.1386	84.40	0.1003	0.1115	75.73	0.0805	0.0945	67.87	0.0652	0.0820
	AdaptiveCP	90.64	0.1291	0.1387	79.87	0.0998	0.1117	71.26	0.0800	0.0946	62.33	0.0648	0.0820
	NexCP	92.91	0.1285	0.1377	83.00	0.1000	0.1114	73.68	0.0796	0.0947	60.87	0.0603	0.0825
	HopCPT	90.82	0.1121	0.1262	77.93	0.0850	0.1037	66.97	0.0672	0.0899	57.70	0.0540	0.0793
	$CACP_{Kmeans}$	90.92	0.0964	0.1121	80.20	0.0721	0.0914	69.17	0.0569	0.0794	59.53	0.0456	0.0708
SPP	$CACP_{KNN}$	91.20	0.0908	0.1065	81.04	0.0692	0.0869	69.68	0.0554	0.0760	60.01	0.0450	0.0683
	$CACP_{Kernel}$	92.77	0.0999	0.1104	82.81	0.0731	0.0883	70.82	0.0572	0.0767	60.04	0.0457	0.0688
	NREL	80.85	0.1389	0.1846	74.93	0.1081	0.1428	68.34	0.0872	0.1194	60.85	0.0708	0.1032
	CQR	89.92	0.1485	0.1815	82.11	0.1106	0.1424	74.73	0.0884	0.1192	65.31	0.0713	0.1030
	AdaptiveCP	89.65	0.1467	0.1800	80.47	0.1102	0.1425	71.86	0.0881	0.1194	61.93	0.0710	0.1032
	NexCP	90.86	0.1500	0.1807	82.33	0.1094	0.1419	70.97	0.0835	0.1190	58.51	0.0633	0.1027
	HopCPT	91.09	0.1255	0.1477	82.36	0.0970	0.1215	72.32	0.0780	0.1054	62.45	0.0634	0.0939
	$CACP_{Kmeans}$	91.77	0.1157	0.1367	82.31	0.0893	0.1134	71.91	0.0719	0.0996	61.46	0.0588	0.0902
	$CACP_{KNN}$	90.78	0.1074	0.1271	82.06	0.0846	0.1066	71.49	0.0692	0.0948	61.17	0.0572	0.0865
	$CACP_{Kernel}$	93.28	0.1165	0.1317	83.06	0.0871	0.1077	72.38	0.0694	0.0948	60.86	0.0566	0.0865

TABLE III: Average Performance across Sites (Day-Ahead Forecasts)

ISO	Method	(1- α) = 90%			(1- α) = 80%			(1- α) = 70%			(1- α) = 60%		
		PICP \uparrow	AIW \downarrow	WS \downarrow	PICP \uparrow	AIW \downarrow	WS \downarrow	PICP \uparrow	AIW \downarrow	WS \downarrow	PICP \uparrow	AIW \downarrow	WS \downarrow
ERCOT	NREL	47.90	0.2072	1.3295	39.39	0.1634	0.8410	33.75	0.1332	0.6469	29.02	0.1087	0.5352
	CQR	90.10	0.4799	0.7095	80.31	0.3593	0.6054	70.22	0.2786	0.5348	60.19	0.2160	0.4788
	AdaptiveCP	72.77	0.3360	0.9910	62.51	0.2573	0.7134	54.65	0.2043	0.5866	47.95	0.1626	0.5051
	NexCP	89.04	0.4676	0.7183	79.34	0.3547	0.6071	69.56	0.2785	0.5347	59.69	0.2180	0.4783
	$CACP_{Kmeans}$	90.09	0.4700	0.6876	80.58	0.3563	0.5859	70.55	0.2808	0.5185	60.60	0.2219	0.4662
	$CACP_{KNN}$	89.56	0.4598	0.6822	80.26	0.3535	0.5785	70.45	0.2816	0.5119	60.68	0.2253	0.4605
	$CACP_{Kernel}$	89.82	0.4621	0.6866	80.62	0.3518	0.5816	70.85	0.2783	0.5134	60.80	0.2209	0.4610
MISO	NREL	71.23	0.2039	0.3404	61.88	0.1609	0.2676	54.05	0.1310	0.2286	46.87	0.1068	0.2012
	CQR	91.16	0.2505	0.3070	81.52	0.1930	0.2545	71.39	0.1543	0.2220	61.13	0.1237	0.1977
	AdaptiveCP	84.85	0.2346	0.3121	73.82	0.1814	0.2589	64.61	0.1458	0.2253	56.01	0.1177	0.1998
	NexCP	89.64	0.2441	0.3048	79.75	0.1893	0.2537	69.84	0.1518	0.2217	59.94	0.1217	0.1975
	$CACP_{Kmeans}$	89.85	0.2281	0.2920	79.74	0.1762	0.2430	69.76	0.1409	0.2134	59.79	0.1129	0.1912
	$CACP_{KNN}$	89.66	0.2227	0.2901	80.13	0.1726	0.2401	70.40	0.1391	0.2104	60.49	0.1127	0.1887
	$CACP_{Kernel}$	90.72	0.2300	0.2899	80.93	0.1770	0.2402	70.75	0.1418	0.2106	60.50	0.1141	0.1889
SPP	NREL	58.76	0.2095	0.8135	49.85	0.1653	0.5422	42.76	0.1346	0.4297	36.54	0.1098	0.3625
	CQR	89.28	0.3647	0.4940	79.14	0.2771	0.4211	69.15	0.2177	0.3701	59.28	0.1729	0.3303
	AdaptiveCP	79.62	0.3028	0.5808	68.33	0.2301	0.4611	58.80	0.1820	0.3924	50.06	0.1454	0.3440
	NexCP	89.41	0.3633	0.4635	79.61	0.2851	0.4033	69.70	0.2270	0.3597	60.01	0.1807	0.3237
	$CACP_{Kmeans}$	89.36	0.3260	0.4173	79.38	0.2621	0.3647	69.18	0.2161	0.3306	58.87	0.1776	0.3041
	$CACP_{KNN}$	89.87	0.3117	0.3868	80.33	0.2564	0.3363	70.07	0.2168	0.3071	59.59	0.1834	0.2863
	$CACP_{Kernel}$	91.04	0.3190	0.3872	81.26	0.2562	0.3346	70.85	0.2136	0.3039	60.27	0.1790	0.2822

B. Conditional Coverage Analysis

This section compares the conditional coverage of the proposed method with baseline approaches across different hours of the day. Fig. 3 shows the PICP for each hour using a target coverage of 80% across all system-level datasets. As illustrated, the proposed method achieves coverage close to

the target across all hours, with slight overcoverage during peak hours and mild undercoverage during non-peak periods. In contrast, baseline methods exhibit substantial miscoverage during early morning and evening hours and provide overconfident intervals during the peak hours. These results highlight the superior adaptability of $CACP$ to distributional shifts

TABLE IV: Comparison of CQR and *CACP* interval widths for MISO system forecasts at 12pm and 6pm. Δ_{IW} indicates the adjustment value applied to the interval width, showing stable CQR intervals and time-varying *CACP* behavior.

Time	α	IW	Δ_{IW} (CQR)	Δ_{IW} (<i>CACP</i>)
12pm	0.1	0.252	0.003	-0.038
	0.2	0.209	0.002	-0.034
6pm	0.1	0.136	0.003	0.002
	0.2	0.106	0.002	0.003

throughout the day. Similar trends are observed for site-level forecasts, but are omitted here due to space constraints.

To further illustrate this adaptive behavior, Fig. 4 shows the distribution of conformity scores for CQR and *CACP*_{KNN} during calibration at two representative hours—6pm and 12 p.m.—on 2019-04-20. Since CQR applies no weighting to conformity scores, the distribution remains unchanged across hours, leading to a fixed small positive adjustment to the prediction intervals (i.e., a uniform increase in width). In contrast, *CACP* uses context-aware weighting, resulting in distinct conformity score distributions for different hours. The initial IW from NREL, and the interval adjustments (i.e., Δ_{IW}) for these two hours are presented in Table IV. At 6pm, a non-peak hour, the weighted conformity scores are concentrated near zero, prompting a small positive adjustment and a slight increase in interval width. At 12 p.m., a peak hour when the initial forecast intervals are already wide, the weighted conformity scores are skewed toward negative values, leading to a reduction in interval width. This adaptive adjustment enables *CACP* to produce more efficient and context-sensitive prediction intervals compared to CQR.

VI. CONCLUSION

This paper introduced *CACP*, a context-aware CP framework for calibrating probabilistic forecasts in renewable energy systems. The proposed method was evaluated against multiple CP baselines for time series forecasting using large-scale datasets from MISO, SPP, and ERCOT, covering both system- and site-level solar generation forecasts provided by NREL. Experimental results showed that *CACP* achieves valid empirical coverage while producing sharper prediction intervals compared to existing baselines. In addition, *CACP* offers a favorable trade-off between predictive performance and computational efficiency, outperforming more resource-intensive methods such as HopCPT. The results highlight the effectiveness of the context-aware weighting mechanism in delivering more reliable conditional coverage. Specifically, the method reduces interval widths in regions where the base forecasts are overconfident and increases them during non-peak hours where underconfidence is more likely, adapting to local uncertainty patterns across time.

Future work will extend this framework by incorporating additional covariates, such as weather data, and by applying it to wind power forecasting. Additional directions include exploring multi-dimensional and hierarchical settings, where context-aware weighting can be combined with the underlying spatio-temporal correlations to enhance forecast reliability.

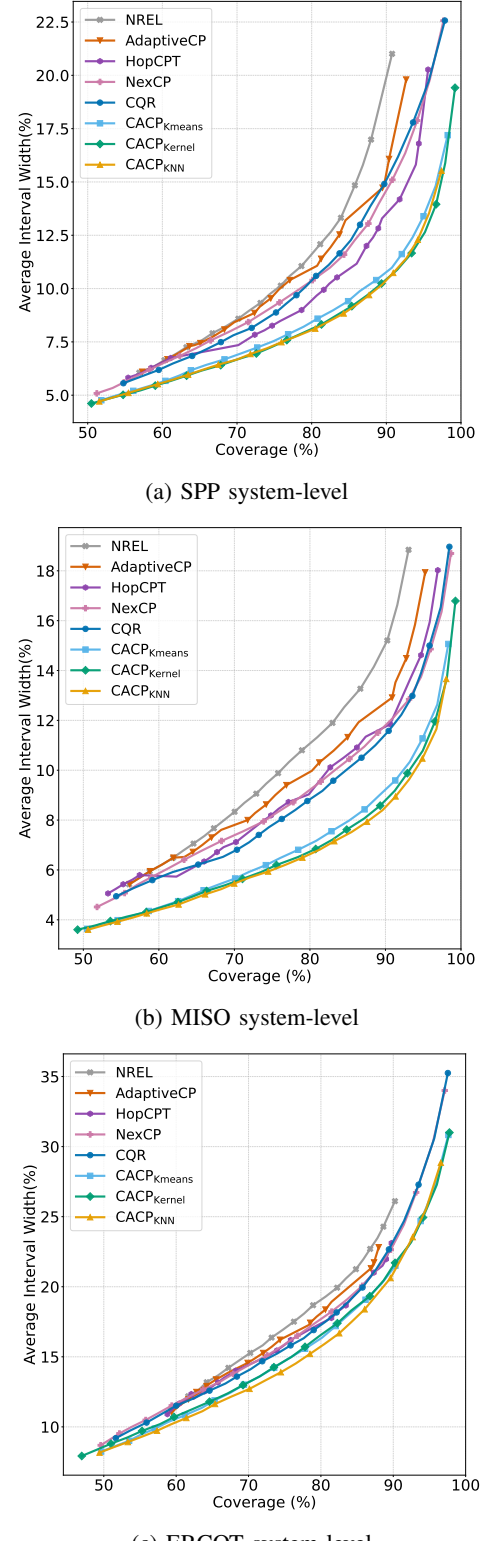
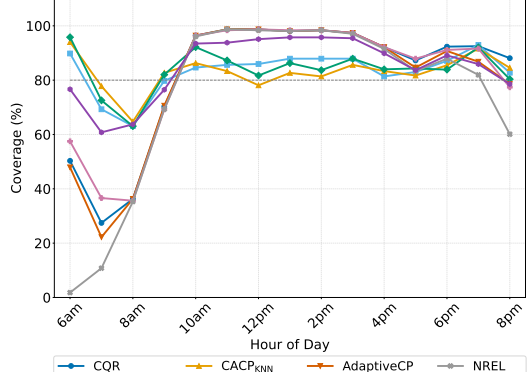
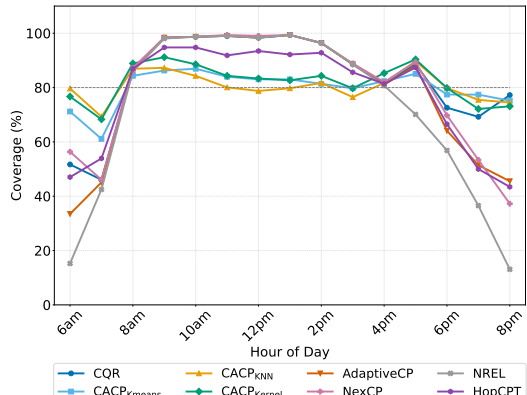


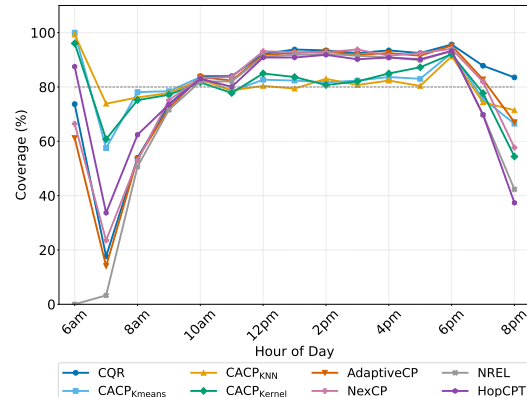
Fig. 2: Coverage vs. AIW trade-off for different CP methods across system-level forecasts in three ISOs. *CACP* methods consistently achieve lower average interval widths compared with baselines at similar coverage rates.



(a) SPP system-level



(b) MISO system-level



(c) ERCOT system-level

Fig. 3: Conditional coverage for different hours of the day across three ISO system-level forecasts (SPP, MISO, and ERCOT) at target marginal coverage 80%. CACP-based methods maintain coverage close to the target across all hours, whereas baseline methods tend to under-cover during early morning and evening periods, and over-cover near midday peak hours.

VII. ACKNOWLEDGMENTS

This work was partially funded by NSF award 2112533 and by Los Alamos National Laboratory’s Directed Research and Development project, “Artificial Intelligence for Mission” (ArtIMis).

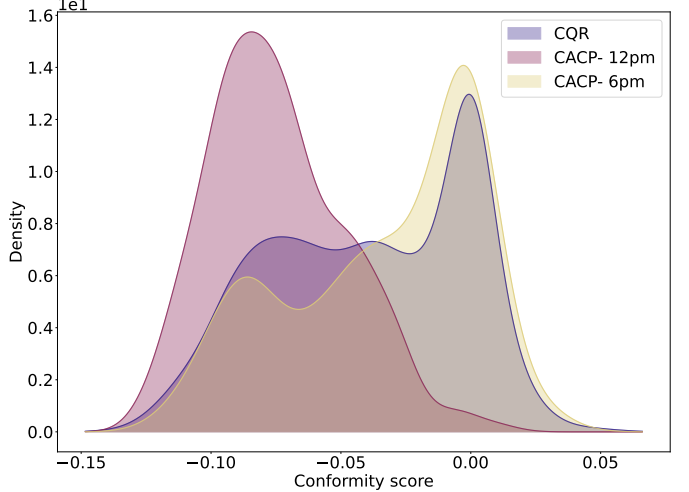


Fig. 4: Distribution of conformity scores for the **MISO system-level** forecasts using CQR and CACP at two representative time steps (12pm and 6pm) on 2019-04-2. While the CQR distribution remains relatively stable across hours, the CACP distribution varies with time, showing a right-skewed (more positive) pattern in the evening (6pm) similar to CQR, and a left-shifted (more negative) distribution at noon (12pm).

REFERENCES

- [1] Andreas Auer, Martin Gauch, Daniel Klotz, and Sepp Hochreiter. Conformal prediction for time series with modern hopfield networks. *Advances in Neural Information Processing Systems*, 36:56027–56074, 2023.
- [2] Rina Foygel Barber, Emmanuel J Candès, Aaditya Ramdas, and Ryan J Tibshirani. Conformal prediction beyond exchangeability. *The Annals of Statistics*, 51(2):816–845, 2023.
- [3] Baiting Chen, Zhimei Ren, and Lu Cheng. Conformalized time series with semantic features. *Advances in Neural Information Processing Systems*, 37:121449–121474, 2024.
- [4] Wei Dong, Xianqing Chen, and Qiang Yang. Data-driven scenario generation of renewable energy production based on controllable generative adversarial networks with interpretability. *Applied Energy*, 308:118387, 2022.
- [5] Kate Doubleday, Stephen Jascourt, William Kleiber, and Bri-Mathias Hodge. Probabilistic solar power forecasting using bayesian model averaging. *IEEE Transactions on Sustainable Energy*, 12(1):325–337, 2020.
- [6] Isaac Gibbs and Emmanuel Candès. Adaptive conformal inference under distribution shift. *Advances in Neural Information Processing Systems*, 34:1660–1672, 2021.
- [7] Tilman Gneiting, Fadoua Balabdaoui, and Adrian E Raftery. Probabilistic forecasts, calibration and sharpness. *Journal of the Royal Statistical Society Series B: Statistical Methodology*, 69(2):243–268, 2007.
- [8] Tilman Gneiting and Matthias Katzfuss. Probabilistic forecasting. *Annual Review of Statistics and Its Application*, 1(1):125–151, 2014.
- [9] Tilman Gneiting, Sebastian Lerch, and Benedikt Schulz. Probabilistic solar forecasting: Benchmarks,

post-processing, verification. *Solar Energy*, 252:72–80, 2023.

[10] Faranak Golestaneh, Pierre Pinson, and Hoay Beng Gooi. Very short-term nonparametric probabilistic forecasting of renewable energy generation—with application to solar energy. *IEEE Transactions on Power Systems*, 31(5):3850–3863, 2016.

[11] Tao Hong, Pierre Pinson, Shu Fan, Hamidreza Zareipour, Alberto Troccoli, and Rob J Hyndman. Probabilistic energy forecasting: Global energy forecasting competition 2014 and beyond, 2016.

[12] Tao Hong, Pierre Pinson, Yi Wang, Rafał Weron, Dazhi Yang, and Hamidreza Zareipour. Energy forecasting: A review and outlook. *IEEE Open Access Journal of Power and Energy*, 7:376–388, 2020.

[13] Jef Jonkers, Diego Nieves Avendano, Glenn Van Wallendael, and Sofie Van Hoecke. A novel day-ahead regional and probabilistic wind power forecasting framework using deep cnns and conformalized regression forests. *Applied Energy*, 361:122900, 2024.

[14] Jonghyeok Lee, Chen Xu, and Yao Xie. Kernel-based optimally weighted conformal prediction intervals. *arXiv preprint arXiv:2405.16828*, 2024.

[15] Wenlong Liao, Zhe Yang, Xinxin Chen, and Yaqi Li. Windgmmn: Scenario forecasting for wind power using generative moment matching networks. *IEEE transactions on artificial intelligence*, 3(5):843–850, 2021.

[16] Weijia Liu, Yangang Liu, Tao Zhang, Yongxiang Han, Xin Zhou, Yu Xie, and Shinjae Yoo. Use of physics to improve solar forecast: Part ii, machine learning and model interpretability. *Solar Energy*, 244:362–378, 2022.

[17] Aleksei Mashlakov, Toni Kuronen, Lasse Lensu, Arto Kaarna, and Samuli Honkapuro. Assessing the performance of deep learning models for multivariate probabilistic energy forecasting. *Applied Energy*, 285:116405, 2021.

[18] Alireza Moradi, Mathieu Tanneau, Reza Zandehshahvar, and Pascal Van Hentenryck. Enhanced renewable energy forecasting and operations through probabilistic forecast aggregation. *arXiv preprint arXiv:2502.07010*, 2025.

[19] Juan M Morales, Antonio J Conejo, Henrik Madsen, Pierre Pinson, and Marco Zugno. Renewable energy sources—modeling and forecasting. In *Integrating Renewables in Electricity Markets: Operational Problems*, pages 15–56. Springer, 2013.

[20] Zhewen Niu, Zeyuan Yu, Wenhua Tang, Qinghua Wu, and Marek Reformat. Wind power forecasting using attention-based gated recurrent unit network. *Energy*, 196:117081, 2020.

[21] Yvet Renkema, Lennard Visser, and Tarek AlSkaif. Enhancing the reliability of probabilistic pv power forecasts using conformal prediction. *Solar Energy Advances*, 4:100059, 2024.

[22] Yaniv Romano, Evan Patterson, and Emmanuel Candes. Conformalized quantile regression. *Advances in neural information processing systems*, 32, 2019.

[23] Brian Sergi et al. ARPA-E PERFORM datasets, 2022.

[24] Zhichao Shi, Hao Liang, and Venkata Dinavahi. Direct interval forecast of uncertain wind power based on recurrent neural networks. *IEEE Transactions on Sustainable Energy*, 9(3):1177–1187, 2017.

[25] Saurabh S. Soman, Hamidreza Zareipour, Om Malik, and Paras Mandal. A review of wind power and wind speed forecasting methods with different time horizons. In *North American Power Symposium 2010*, pages 1–8, 2010.

[26] Saurabh S Soman, Hamidreza Zareipour, Om Malik, and Paras Mandal. A review of wind power and wind speed forecasting methods with different time horizons. In *North American power symposium 2010*, pages 1–8. IEEE, 2010.

[27] Conor Sweeney, Ricardo J Bessa, Jethro Browell, and Pierre Pinson. The future of forecasting for renewable energy. *Wiley Interdisciplinary Reviews: Energy and Environment*, 9(2):e365, 2020.

[28] Rosemary Tawn and Jethro Browell. A review of very short-term wind and solar power forecasting. *Renewable and Sustainable Energy Reviews*, 153:111758, 2022.

[29] Ryan J Tibshirani, Rina Foygel Barber, Emmanuel Candès, and Aaditya Ramdas. Conformal prediction under covariate shift. *Advances in neural information processing systems*, 32, 2019.

[30] Vladimir Vovk, Alexander Gammerman, and Glenn Shafer. *Algorithmic learning in a random world*, volume 29. Springer, 2005.

[31] Wei Wang, Bin Feng, Gang Huang, Chuangxin Guo, Wenlong Liao, and Zhe Chen. Conformal asymmetric multi-quantile generative transformer for day-ahead wind power interval prediction. *Applied Energy*, 333:120634, 2023.

[32] Yun Wang, Runmin Zou, Fang Liu, Lingjun Zhang, and Qianyi Liu. A review of wind speed and wind power forecasting with deep neural networks. *Applied energy*, 304:117766, 2021.

[33] Min Xia, Haidong Shao, Xiandong Ma, and Clarence W De Silva. A stacked gru-rnn-based approach for predicting renewable energy and electricity load for smart grid operation. *IEEE Transactions on Industrial Informatics*, 17(10):7050–7059, 2021.

[34] Yuying Xie, Chaoshun Li, Mengying Li, Fangjie Liu, and Meruyert Taukenova. An overview of deterministic and probabilistic forecasting methods of wind energy. *Iscience*, 26(1), 2023.

[35] Chen Xu and Yao Xie. Conformal prediction interval for dynamic time-series. In *International Conference on Machine Learning*, pages 11559–11569. PMLR, 2021.

[36] Chen Xu and Yao Xie. Conformal prediction for time series. *IEEE transactions on pattern analysis and machine intelligence*, 45(10):11575–11587, 2023.

[37] Chen Xu and Yao Xie. Sequential predictive conformal inference for time series. In *International Conference on Machine Learning*, pages 38707–38727. PMLR, 2023.

[38] Qianyao Xu, Dawei He, Ning Zhang, Chongqing Kang, Qing Xia, Jianhua Bai, and Junhui Huang. A short-term wind power forecasting approach with adjustment of numerical weather prediction input by data mining.

IEEE Transactions on sustainable energy, 6(4):1283–1291, 2015.

[39] Hanyu Zhang, Reza Zandehshahvar, Mathieu Tanneau, and Pascal Van Hentenryck. Weather-informed probabilistic forecasting and scenario generation in power systems. *Applied Energy*, 384:125369, 2025.

[40] Yao Zhang, Jianxue Wang, and Xifan Wang. Review on probabilistic forecasting of wind power generation. *Renewable and Sustainable Energy Reviews*, 32:255–270, 2014.